ACS APPLIED POLYMER MATERIALS



pubs.acs.org/acsapm
Article

# Mechanically Robust and Biodegradable Electrospun Membranes Made from Bioderived Thermoplastic Polyurethane and Polylactic Acid

Robert J. Chambers, Bhausaheb S. Rajput, Gordon B. Scofield, Jaysen Reindel, Katherine O'Shea, Richey Jiang Li, Ryan Simkovsky, Stephen P. Mayfield, Michael D. Burkart, and Shengqiang Cai*

Cite This: ACS Appl. Polym. Mater. 2024, 6, 12528−12537



**ABSTRACT:** Petroleum-based plastic waste plagues the natural environment, but plastics solve many high-performance solutions across industries. For example, porous polymer membranes are used for air filtration, advanced textiles, energy, and biomedical applications. Sustainable and biodegradable Bioplastic membranes can compete with nonrenewable materials in strength, durability, and functionality but biodegrade under select conditions after disposal. Membranes electrospun using a blend of bioderived thermoplastic polyurethane (TPU) and polylactic acid (PLA) perform effectively under tensile and cyclic loading, act adequately as an air filter media, and biodegrade in a home-compost environment, with the aliphatic formulation of TPU showing greater biodegradability compared to the formulation containing aromatic moieties. Blending TPU with PLA dramatically increases the strain at break of the PLA membrane, while the addition of PLA in TPU stiffens the material considerably. Measurements of the pressure drop and filtration efficiency deem this electrospun membrane an effective air filter. This membrane provides a solution to the need for quality air filtration while decreasing the dependence on petroleum feedstocks and addressing the issue of plastic disposal through biodegradation.

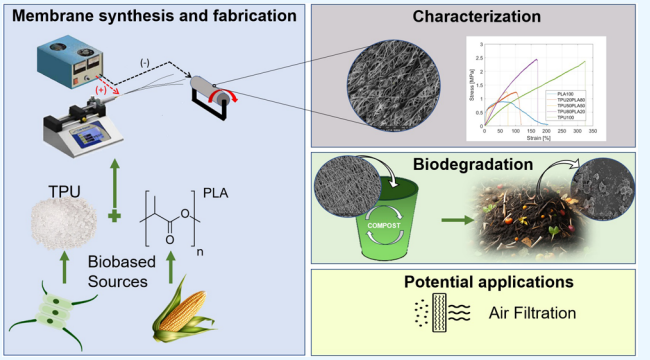


**KEYWORDS:** *biodegradable polymer, sustainable materials, air filtration, biobased polyester polyol, electrospun membrane, mechanical testing*

## INTRODUCTION

Society needs materials to perform their intended function while limiting the negative effects during synthesis, use, and disposal. The versatility of plastics makes them suitable for a range of applications. Controlling the chemical composition and physical structure of the plastic alters the flexibility, hydrophobicity, or permeability of the final product. Unfortunately, petroleum-derived, nonbiodegradable plastics burden the environment with greenhouse gas emissions and persistent plastic waste. Petroleum extraction and processing accounts for 30% of $CO_2$ emissions per year.[1] Annual plastic production has reached over 380 million metric tons and increases at a rate of 4% annually; generating 6.3 billion tonnes of plastic waste since 1950. With a 9% recycling rate, the majority of plastic enters landfills or the natural environment after its intended use.[2] This waste is accumulated in places like the Great Pacific Garbage Patch, covering an area of 1.6 million square kilometers.[3] Plastics produced from bioderived sources that readily biodegrade simultaneously reduce the dependence on fossil fuels and the accumulation of polymer waste and microplastics after disposal. Biological sources for plastics include plant sugars, algal sugars, and oils, as well as nonedible lignocellulosic biomass.[4] It is important to note that bioderived plastics, often referred to as bioplastics, are not inherently biodegradable. Biodegradation refers to the conversion of material into biomass and $CO_2$ due to microbial activity. Many plastics that claim to be biodegradable require industrial-grade composting environments, where high temperatures and active monitoring of compost conditions facilitate biodegradation. When left in conventional residential compost, some plastics persist.[5] Other common disposal environments (marine, aquatic, and landfills) have different temperatures and microorganismal profiles that influence biodegradation rates. Polylactic acid (PLA), for example, is known to biodegrade rapidly under industrial composting conditions but does not appear to biodegrade in home compost

Received: June 25, 2024
Revised: October 3, 2024
Accepted: October 4, 2024
Published: October 16, 2024

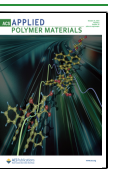

and marine environments.[6,7] Royer et al. observed no sign of biodegradation of PLA placed in the ocean after over 400 days.

Unfortunately, the facile processing and low-cost nature of plastics drive their use in single-use applications. The amount of resources consumed by the production of single-use plastics and the subsequent environmental impacts far outweighs the duration of use. Driven by health concerns during the COVID-19 pandemic, filtration face masks provided protection from airborne pathogens, but generated substantial waste upon disposal.[8] Air filtration is crucial for maintaining healthy indoor or personal air quality by removing airborne pollutants such as particulate pollution, dust, allergens, mold spores, bacteria, and viruses that can cause a range of health problems. Filtration systems work by trapping these particles and preventing them from circulating in the air.[9,10] One practical way to process polymers into filtration membranes is electrospinning.

In electrospinning, an electric field produces very fine fibers from a polymer solution or melt. This facile process produces fibrous membranes with tunable porosity and fiber diameter by modifying several key process parameters, such as solution concentration, flow rate, applied voltage, collector speed, and collector distance. This fibrous architecture can be applied to a range of applications, including tissue scaffolds, wound care, liquid filtration, acoustic materials, energy, air filtration, and advanced textiles.[11,12]

Liu et al. tested a variety of electrospun polymers such as polyacrylonitrile, polyvinylpyrrolidone, polystyrene, poly(vinyl alcohol), and polypropylene.[13] They applied their polyacrylonitrile filters in a Beijing field test and found a removal efficiency of 98.69%. While highly effective as filters, no mechanical strength information was published on petroleum-based membranes. Under cyclic wind loading, the fibers could fracture and reduce the filtration efficiency. Biobased electrospun membranes can be produced from materials like cellulose, chitosan, cyclodextrin, and lignin, but often require extra processing steps or cospinning with another polymer to generate a functional filter, but the mechanical properties of these biopolymer membranes struggle to reach the function specifications associated with of pure polymer membranes.[14,15] Additionally, studies often claim that these membranes are biodegradable without demonstrating the biodegradation process. As an example, the biobased polymer PLA has been used for filtration membranes, but the brittle nature of PLA makes it susceptible to fiber fracture and reduction in filtration efficiency.[16−18] Plasticizers, like PVA, or strengthening constituents, like cellulose nanocrystals, can be added to the polymer solution during electrospinning to make more mechanically robust filters, but this can hinder biodegradation or processing conditions.[19,20] Blending PLA with a more ductile material like thermoplastic polyurethane (TPU) improves the elongation at break and tensile strength of the electrospun membranes by over 250%.[21,22] TPU alone has been shown to make robust air filters.[23−25] The majority of TPUs are petroleum-based and nondegradable. However, polyurethane can be synthesized from biobased sources and can biodegrade through natural pathways. Not all polyurethane biodegrades equally. Polyester urethane biodegrades much more readily compared with polyether urethane. Even within polyester urethane, the degradation behavior can vary based on the monomers used in synthesis and the microorganisms present in the compost environment.[26−28] The different polyols and diisocyanates used during the synthesis result in TPUs with varying aromatic and aliphatic structures in the repeat units of the polymer. Stiff aromatic rings can increase strength and stiffness but may hinder biodegradation.[29,30] We hypothesized that blending PLA with bioderived and biodegradable TPUs improves the mechanical properties of electrospun PLA membranes while enabling biodegradation under home composting conditions. We test the hypothesis by electrospinning two different polyester urethane formulations blended with PLA. Both TPUs used to test this hypothesis have a biobased carbon percentage of over 60%.

## EXPERIMENTAL METHODS

**Materials.** Chloroform ($CHCl_3$; Sigma-Aldrich; HPLC grade) and dimethylformamide (DMF; Sigma-Aldrich, 99.8%) were used as received without further purification. The PLA (3100HP Ingeo) was purchased from NatureWorks. The polyester-polyol SaSbPDO with 1500 g/mol molecular weight was prepared following the literature method with some modifications.[26,27] For the polyol synthesis, bioderived sebacic acid (98%, biobased) was supplied by Acros Organics, and biobased succinic acid was purchased from Visolis. The biobased 1,3-propanediol was received from Susterra and used as received for polyol and TPU synthesis. The aliphatic biobased thermoplastic polyurethane was supplied by Algenesis Corporation and used as received.

**Methods.** *Polyester-Polyol SaSbPDO1500 Synthesis.* Polyester-polyol synthesis was performed in a 500 mL three-neck round-bottom flask equipped with a reflux condenser, Dean−Stark apparatus, and a heating metal block in a hot plate. The calculated amounts of diacids, such as succinic acid (142.2 g, 1.20 mol), sebacic acid (81.2 g, 0.40 mol), and 1,3-propanediol (134.4 g, 1.77 mol), were added under a nitrogen atmosphere. The polycondensation was started at 150−160 °C; subsequently, the temperature increased to 170−180 °C for 1 h. The rapid release of water byproduct was observed in an initial 4−5 h. Afterward, the DBTDL catalyst was added when 80−90% water was collected, and the reaction ran for approximately 2−3 days until the desired acid and hydroxyl number was achieved. The polyester-polyol SaSbPDO1500 showed an acid number of 1.3 mg of KOH/g and a hydroxyl number of around 75 mg of KOH/g, as determined by the appropriate acid and hydroxyl titrations.

*Synthesis of TPU.* Before the TPU reaction, polyester-polyol and chain extender were dried in the vacuum oven for 24 h at 90 °C. The SaSbPDO1500 polyester-polyol (46.7 g, 0.030 mol) and 1,3-propanediol (4.5 g, 0.060 mol) were combined into a plastic cup and heated to 75 °C. The polyol mixture was mixed using a speed mixer (FlackTek) at 2000 rpm for 1 min to make homogeneous and eliminate bubbles from the polyol mixture. In another glass container, 4,4′-methylenediphenylene diisocyanate (MDI, 24.8 g, 0.099 mol) was heated to 75 °C until liquid. The liquid MDI was then added into the polyol mixture and mixed at 2000 rpm for approximately 20 s. Exothermic reactions were observed after mixing with the diisocyanate. Finally, the polymer mixture was immediately poured into a Teflon mold before a gel point and cured at 80 °C for 2 h and 100 °C for 20 h to achieve a sheet or film product. Following ASTM D638, a dog-bone-shaped cutting die was used to make sample specimens for tensile strength and elongation at break measurement.

*Electrospinning Solution Preparation.* The PLA solution was made by adding 1 g of PLA pellets in 10 g of $CHCl_3$ in a vial and stirring overnight, yielding a 10 wt % solution. The aromatic TPU solution was made by adding 1 g of TPU pellets into 10 g of DMF in a vial and stirring overnight, yielding a 10 wt % solution. The aliphatic TPU required a 20 wt % loading in DMF to properly electrospin. The TPU and PLA pellets were dried under a vacuum at 50 °C for 12 h before use. After the solutions of PLA/$CHCl_3$ and TPU/DMF were created, the mass ratios of 100, 80, 50, 20, and 0% TPU were made in a vial and mixed for 1 h before loading into the syringe for electrospinning. The solution was electrospun directly after mixing to minimize the phase separation in the blended solutions. These membranes were called TPU100, TPU80PLA20, TPU50PLA50, TPU20PLA80 and PLA100, respectively.

*Electrospinning Process.* The solutions were loaded into a 3 mL syringe with an 18 gauge blunt needle tip. This syringe tip had an


https://doi.org/10.1021/acsapm.4c01974
ACS Appl. Polym. Mater. 2024, 6, 12528−12537

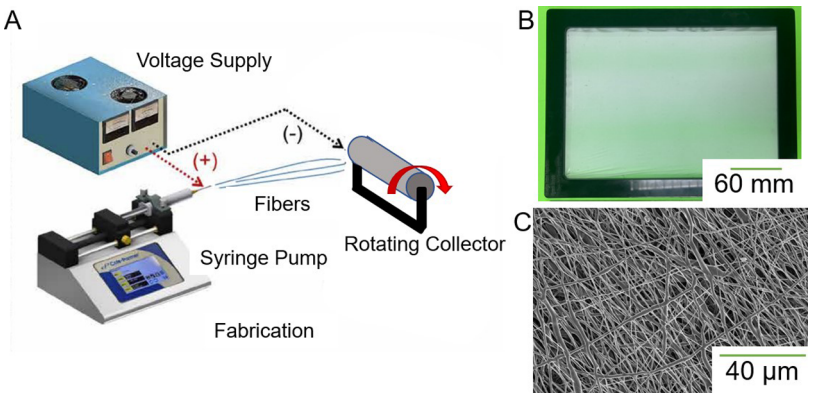


**Figure 1.** Electrospinning setup and resulting fiber architecture. (A) Schematic of the electrospinning setup. (B) Optical image of an electrospun TPU membrane with a 60 mm scale bar (C) Scanning Electron Microscope (SEM) image of electrospun TPU with 40 $\mu$m scale bar.

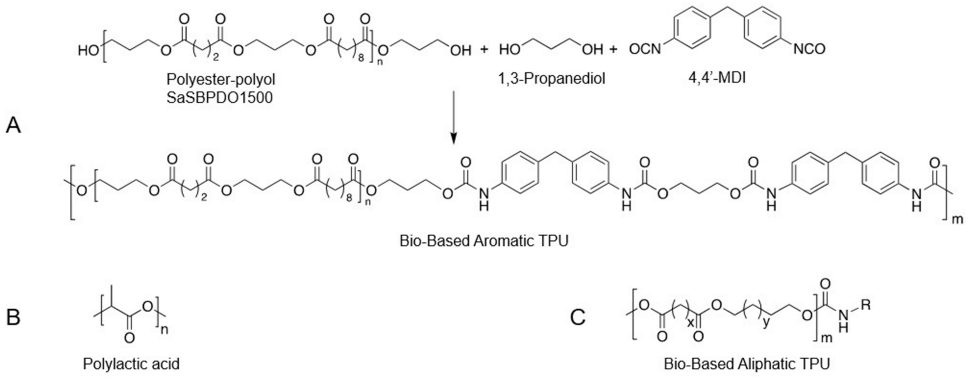


**Figure 2.** Chemical structure of polymers. (A) Synthesis of biobased aromatic TPU used in electrospinning. (B) Monomer structure of PLA. (C) General structure of Algenesis aliphatic TPU.

internal diameter of 0.838 mm. A syringe pump (Cole-Parmer) was used to precisely control the flow rate from the needle with a speed of 1 mL/h. A rotating collector placed 12 cm from the nozzle tip captured the electrospun fibers. The collector was spun at approximately 900 rpm. The positive electrode of the power source was connected to the tip of the needle; the negative electrode of the power source was connected to the metal mesh. The applied voltage was set to 9 kV. This setup can be seen in Figure 1A.

**Characterization.** *Nuclear Magnetic Resonance.* $^{1}$H NMR and $^{13}$C NMR spectra of the biobased TPU were recorded on a JEOL 500 MHz spectrometer. The resulting spectra are included in the Supporting Information.

*Differential Scanning Calorimetry (DSC).* The differential scanning calorimetry (DSC) analysis was completed using a TA Instruments from −120 to 220 °C at the rate of 10 °C/min under a nitrogen atmosphere. The heating curves were used to determine the glass transition temperature ($T_g$) and melting temperature ($T_m$) for the bulk TPUs. The data was recorded from the third heating cycle and is provided in the Supporting Information.

*Electrospinning Solution Viscosity.* A rheology experiment on the PLA and TPU solutions was performed to compare the viscosity of the spinning solutions within a probable shear-rate range. The experiment was performed on a TA Instruments Discovery HR 20. A flow sweep was performed from shear rates of 1−100 s$^{-1}$. A 60 mm cone geometry with a 55 $\mu$m truncation gap was used. Three replicates were tested for each solution.

*Membrane Morphology.* The fiber morphology of the electrospun membranes was measured with a scanning electron microscope (SEM, FEI Apreo). Before imaging, the samples were sputter-coated with iridium for 60 s to improve visibility. The average fiber diameter was measured using ImageJ. The fiber diameter was measured across 50 measurements.

*Mechanical Testing.* The uniaxial tension tests were performed on a Universal Mechanical Testing System (5965 Dual Column Testing System, Instron) with a 1 kN load cell, following ASTM D882. Rectangular samples (20 mm × 10 mm) were adhered to acrylic plates and held between tensile grippers. The thickness of the sample was measured in three locations on the sample using a digital micrometer and averaged (Mitutoyo 293-721-30). Five replicates of each variety were tested. The crosshead speed was 10 mm/min, which corresponds to a strain rate of 50% min$^{-1}$.

The cyclic tension tests were performed on a dynamic test system (Electroforce 3300, TA Instruments). The specimens had a pure shear geometry to increase the load to a measurable range. The width of the specimens was 60 mm, and the height was 10 mm. The thickness was measured using the same method as that for the tensile test. The specimens were stressed in a sawtooth motion to 50% strain at a frequency of 0.1 Hz for 1000 cycles. This corresponds to a strain rate of 600% min$^{-1}$.

*Biodegradation Testing.* Samples were placed on clean glass slides and then placed in a controlled compost environment. The compost was collected from Roger's Community Garden at the University of California San Diego. The compost environment was controlled at a temperature of 45 °C and 75−85% relative humidity. Portions of the samples were removed at select time points and imaged with SEM to observe degradation of the fibers. The glass slide was fractured to remove a section for imaging. Optical images of the degraded membranes are included in the Supporting Information. FTIR spectra of the degraded membranes were recorded with a Nicolet i520 FTIR spectrometer. The FTIR spectra were collected over 16 scans from 700 to 3700 cm$^{-1}$.

For a demonstration of degradation, a 3 cm by 4 cm aliphatic TPU membrane was adhered to an acrylic frame. The compost environment was similar to the controlled setup used in the earlier experiment. An


https://doi.org/10.1021/acsapm.4c01974
ACS Appl. Polym. Mater. 2024, 6, 12528−12537

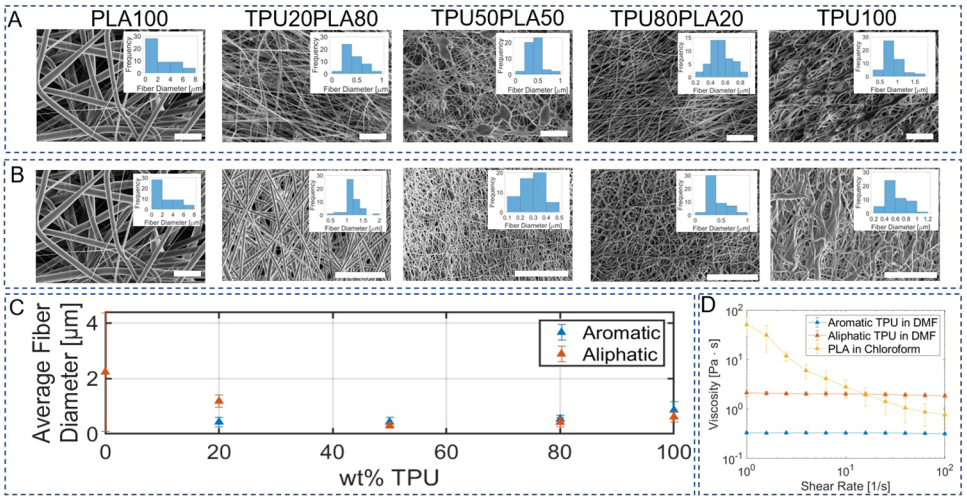


**Figure 3.** Fiber blend morphology. (A) SEM images at 1600× magnification of PLA and aromatic TPU electrospun blends. Scale bars are 20 $\mu$m. (B) SEM images at 1600× magnification of PLA and aliphatic TPU electrospun blends. (C) Average fiber diameter versus weight percentage of TPU in the blend. Error bars denote one standard deviation across the 50 measurements per membrane. (D) Steady-state shear-rate dependence of viscosity for spinning solutions.

optical image was taken three times a day and stitched into a time-lapse. This video is included in the Supporting Information.

**Air Filtration Quality Testing.** *Air Permeability.* Air Permeability was measured following the ASTM D737. The membrane was clamped in a test head with a circular test area of 38.3 $cm^2$. A digital manometer (Keller LEX1) was used to measure the up and downstream air pressure of the membrane. An analog flow meter measured the air velocity through the test area.

*Filtration Efficiency.* The filtration efficiency was measured by generating aerosol particles upstream of the filter membrane, providing a pressure difference across the membrane and measuring particle concentration downstream of the membrane using a particulate matter sensor. Burning tissue paper was used as a particulate matter source. The digital manometer was used to measure the pressure drop across the membrane. The filter efficiency was calculated using eq 1:

$$\eta = \frac{C_{up} - C_{down}}{C_{up}} \quad (1)$$

where $C_{up}$ and $C_{down}$ are the PM concentrations up and downstream of the membrane, respectively. The quality factor is an overall metric of the filtration performance. It is calculated using eq 2:

$$QF = \frac{-\ln(1-\eta)}{\Delta P} \quad (2)$$

where $\Delta P$ is the pressure drop across the membrane.

## RESULTS AND DISCUSSION

**Biobased Aromatic TPU Synthesis.** The polyester-polyol SaSbPDO1500, chain extender 1,3-propanediol, and 4,4-methylenedipheylene diisocyanate were combined in a molar ratio of 1:2:3.1 to achieve an isocyanate index of 1.1 isocyanate index. The prepared TPU has a calculated biocarbon content of up to 67%. This chemical reaction is shown in Figure 2A. Since the functionality of all the constituents is two and the polymer forms a transparent solution when placed in DMF no network formation has occurred. This material is considered a thermoplastic and not a thermoset. The formation of TPU was confirmed by $^1$H and $^{13}$C NMR (Figures S2 and S3). The $^1$H peak at 9.51 ppm corresponds to the urethane proton (−NH), confirming that the polyurethane reaction occurred between the polyol mixture and isocyanate. Peaks between 7.04 and 7.31 ppm originate from aromatic protons from the diphenyl rings. In the $^{13}$C NMR spectrum, the resonance at 154 ppm is the characteristic peak of a urethane carbonyl carbon (−NHCO). The peaks at 172.4 and 173.4 ppm correspond to the polyol-based ester carbonyl carbon. The biobased aromatic TPU displayed a $M_n$ and $M_w$ of 117,000 and 297,000 g/mol respectively with 2.50 PDI (Figure S1). The mechanical properties of TPU were determined by a Universal Testing Machine (UTM) with a strain rate of 50 mm/min using an ASTM D638. The biobased aromatic TPU presented a 32 MPa tensile strength and 880% elongation at break (Figure S4A). The TPU displayed a $T_g$ and $T_m$ of −28.5 and 181 °C, respectively (Figure S5). The TPU showed a shore A hardness in the range of 85−87. When this polymer is placed in DMF for electrospinning it is fully soluble and forms a transparent solution.

For comparison, tensile tests were conducted on the aliphatic TPU provided by Algenesis. Bulk aliphatic TPU had an average tensile strength of 30.9 ± 1.6 MPa and elongation at break of 1014 ± 25% (Figure S4B). This difference could be due to the presence of rigid polymer chains of MDI in the biobased aromatic TPU, which might increase the intermolecular force that includes strong hydrogen bonding between urethane and ester groups, resulting in the higher strength compared to biobased aliphatic TPU. Often there is a trade-off between strength and elongation. These materials in the bulk form demonstrate that trade-off.

**Characterization of Electrospun Membrane.** *Mechanical Testing.* The nano- and microstructures of a permeable membrane influence the potential applications of the membrane. In electrospun membranes, the fiber diameter and membrane thickness dictate the porosity, which drives the permeability of the material. The fiber architecture also influences other key properties, such as mechanical strength and filtration efficiency. In electrospinning, several material and process parameters interact to form the polymer jet, which ultimately defines the resulting fiber diameter. Of these parameters, volumetric charge density, distance from the nozzle to the collector, initial jet/orifice radius, relaxation time, and viscosity have the strongest effect on fiber size. Other parameters such as initial polymer concentration, solution density, electrical potential, and solvent vapor pressure play as part of polymer jet


https://doi.org/10.1021/acsapm.4c01974
ACS Appl. Polym. Mater. 2024, 6, 12528−12537

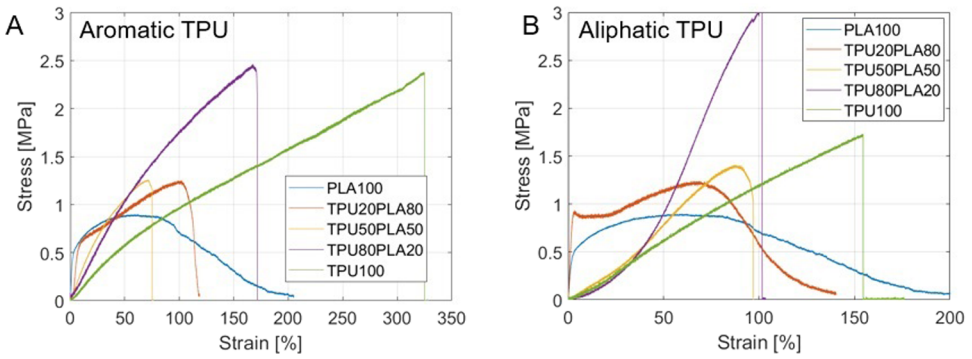


**Figure 4.** Summary of mechanical behavior. Tensile testing of electrospun TPU and PLA blends with a strain rate of 50% per minute. Specimen geometry of 20 mm × 10 mm was used in tensile testing. (A) Aromatic TPU and PLA blends. (B) Aliphatic TPU and PLA blends.

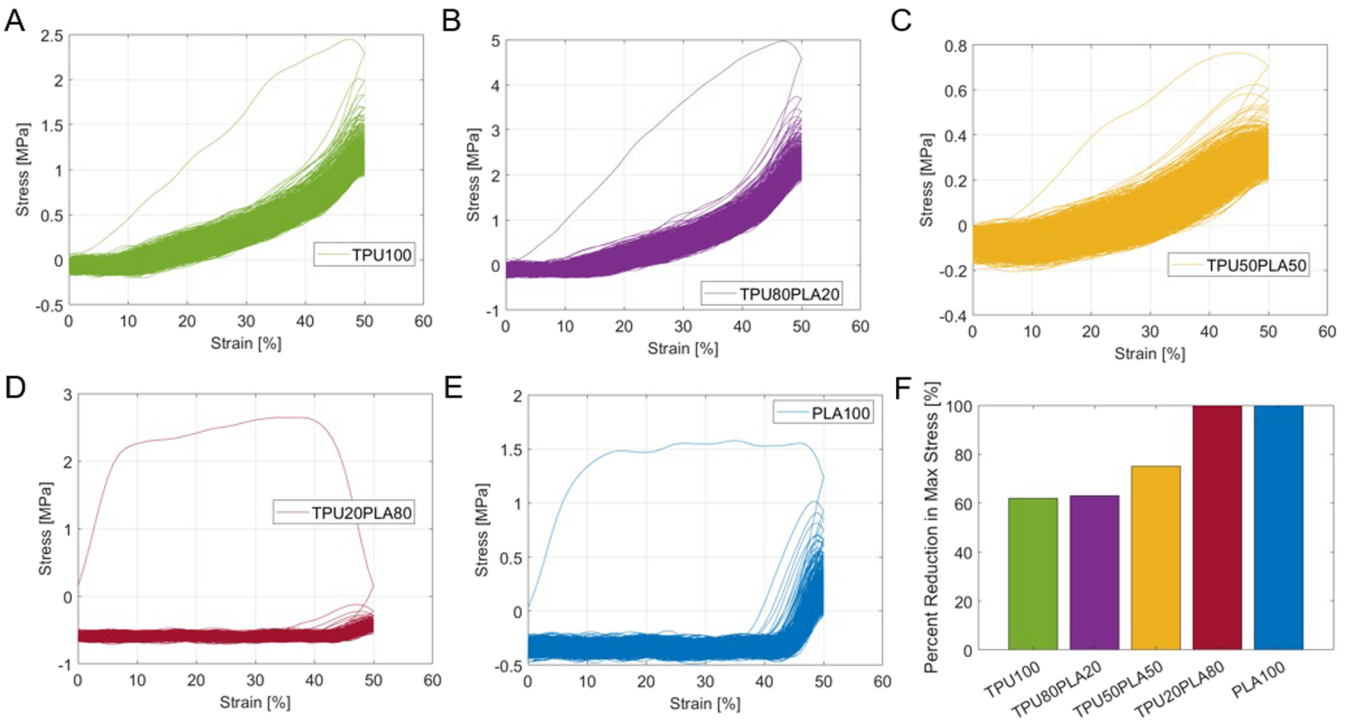


**Figure 5.** Cyclic testing of PLA and aromatic TPU blends. Results from 1000 cycles to 50% strain at a frequency of 0.1 Hz. Pure shear specimen geometry of 10 mm × 60 mm was used for (A) TPU100, (B) TPU80PLA20, (C) TPU50PLA50, (D) TPU20PLA80, and (E) PLA100. (F) Reduction in maximum stress from the first to last cycle.

formation as well.[31] In this study, the spinning parameter was kept constant, and the fiber architectures were observed with SEM, as shown in Figure 3. The weight percentage of TPU to PLA in the solution was the controlled variable. Based on these fixed spinning parameters, the fiber diameter of pure TPUs and the TPU-PLA blends varied from 0.29 to 1.2 $\mu$m, as compared to the pure PLA fiber diameter of 2.14 $\mu$m. As the TPU concentration increased, the melding of fibers occurred, causing the individual fibers to appear less defined and the porosity of the membrane to decrease. One potential material parameter to explain PLA fiber's larger diameter is solution viscosity, shown in Figure 3D. Within this shear-rate range, the PLA solution exhibited shear thinning behavior, whereas the viscosity of the TPU solutions was near constant. The higher viscosity at lower shear rates of the PLA solution could be one of the factors that influence larger average fiber size. The lower viscosity of the aromatic TPU compared with the aliphatic TPU could be due to the lower polymer concentration in this solution. The polymer concentration of the aliphatic TPU had to be higher to form a homogeneous fibrous membrane. At polymer concentrations below 20 wt % electrospinning was unsuccessful for the aliphatic TPU. Further parameter modification could be done to tailor fiber geometry and porosity for intended membrane applications.

In its bulk form, PLA is a relatively brittle polymer. Common elongation at break values is 2%. The near-random orientation of fibers resulting from electrospinning allowed for relative movement between PLA fibers and a significant increase in elongation before fracture in an electrospun membrane, as shown in Figure 4. Single fibers have strain at break comparable to the bulk material, but the macro-scale response of the fibrous mat exhibits a softer and more ductile behavior.[19] Additionally, the PLA fibers fractured in a slowly cascading nature, unlike the rapid fracture of bulk PLA. When cyclically loaded, the load-carrying capacity of PLA is near zero after one cycle due to


https://doi.org/10.1021/acsapm.4c01974
ACS Appl. Polym. Mater. 2024, 6, 12528−12537

**Table 1. Mechanical Properties of the TPU Electrospun Membranes**[a]

| material | $E$ [MPa] | UTS [MPa] | $\epsilon_{frac}$ [%] | toughness [MPa/m$^{-3}$] |
|---|---|---|---|---|
| PLA100 | 25.2 ± 5.5 | 0.85 ± 0.07 | 74 ± 19 | 0.99 ± 0.26 |
| TPU20PLA80 | 10.0 ± 2.0 (21.0 ± 4.0) | 0.87 ± 0.08 (1.16 ± 0.24) | 103 ± 11 (86 ± 11) | 0.66 ± 0.11 (1.03 ± 0.17) |
| TPU50PLA50 | 2.6 ± 0.38 (2.0 ± 0.3) | 1.06 ± 0.14 (1.09 ± 0.42) | 68 ± 11 (109 ± 22) | 0.44 ± 0.12 (0.91 ± 0.57) |
| TPU80PLA20 | 2.4 ± 0.3 (0.7 ± 0.1) | 3.05 ± 0.25 (2.59 ± 0.71) | 203 ± 20 (136 ± 45) | 3.73 ± 0.56 (1.51 ± 0.49) |
| TPU100 | 1.0 ± 0.08 (1.0 ± 0.29) | 2.18 ± 0.30 (1.35 ± 0.34) | 344 ± 23 (144 ± 22) | 4.15 ± 0.74 (0.71 ± 0.37) |

[a]Note: Properties in parentheses are from aliphatic TPU blends. The properties outside the parentheses are from aromatic TPU blends. One standard deviation is denoted after the average value of each property from the five specimens of all varieties tested. The individual stress/strain curves for each specimen are provided in Figures S6 and S7.

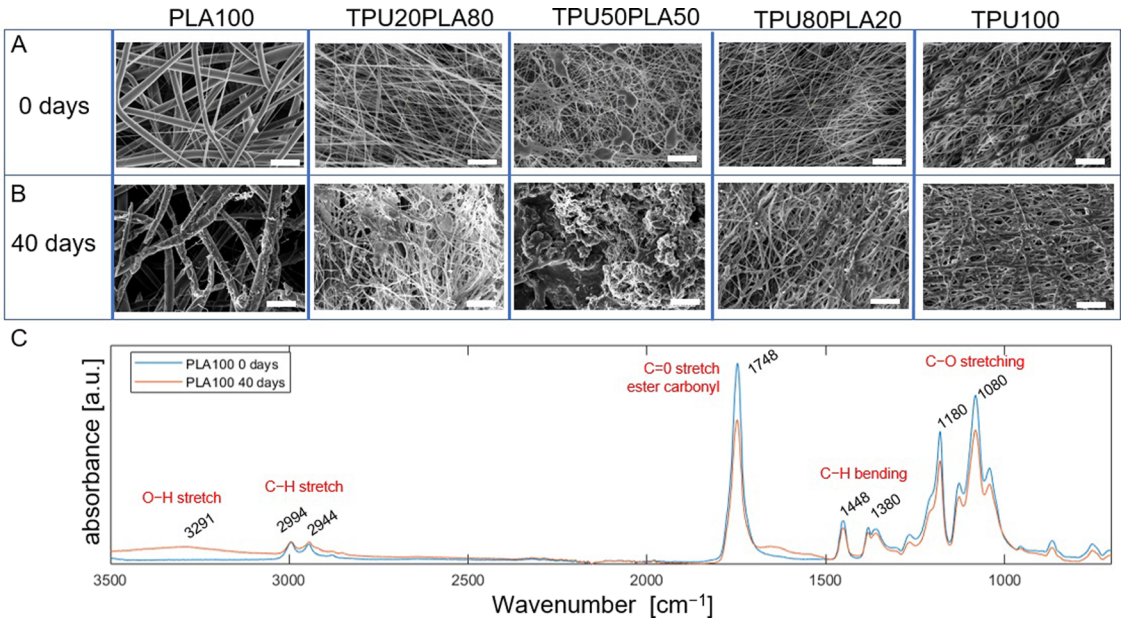


**Figure 6.** Degradation of aromatic TPU blends. SEM images of PLA and aromatic TPU blend membranes (A) before and (B) after 40 days of incubation in a home compost environment (45 °C and 75−85% relative humidity). All scale bars are 20 $\mu$m. (C) FTIR spectra of the PLA membrane before and after 40 days of incubation buried in compost.

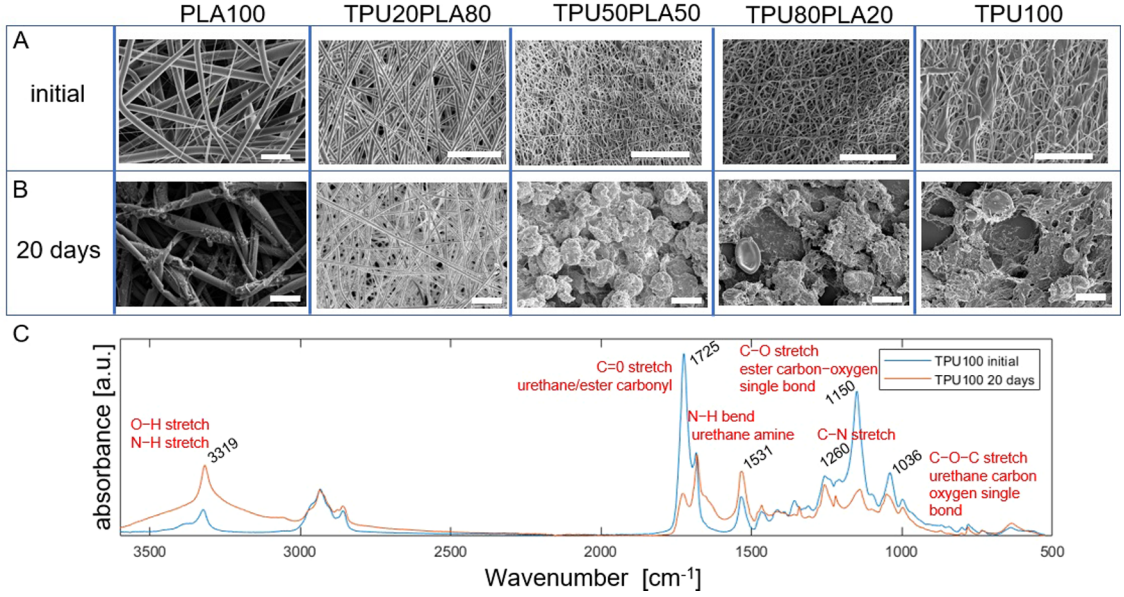


**Figure 7.** Degradation of aliphatic TPU blends. SEM images of PLA and aliphatic TPU blend membranes (A) before and (B) after 20 days of incubation in a home compost environment (45 °C and 75−85% relative humidity). All scale bars are 20 $\mu$m. (C) FTIR spectra of the aliphatic TPU membrane before and after 20 days of incubation buried in compost.



https://doi.org/10.1021/acsapm.4c01974
ACS Appl. Polym. Mater. 2024, 6, 12528−12537

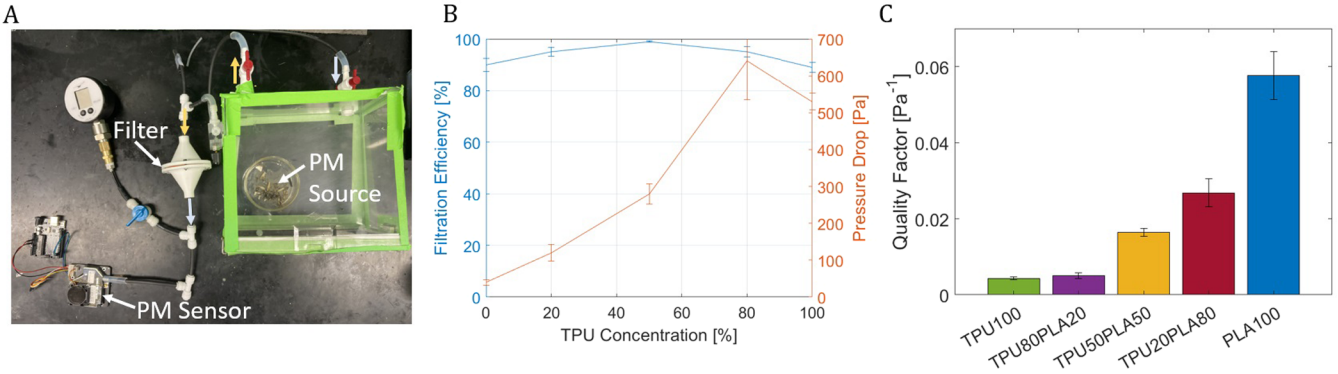


**Figure 8.** Application of electrospun membrane in air filtration. (A) Image of the experimental setup. (B) Filtration efficiency and pressure drop of the TPU/PLA blends. Pressure drop is measured at a flow rate of 10 L/min. (C) Quality factor of the air filtration membranes.

slippage and breakage of individual fibers without complete membrane failure, as shown in Figure 5.[32]

TPU can often exhibit highly elastic and stretchable tensile properties. This elastic behavior is maintained in electrospun membranes. Pure aromatic TPU membranes fractured at an average of 344%, with a stress at a fracture of 2.1 MPa (Figure 4A). The aliphatic TPU had slightly lower elongation at break and ultimate tensile strength (UTS), measured at 144% and 1.35 MPa, respectively. This deviation from bulk properties could be due to several factors, such as differences in fiber architecture, fiber−fiber fusion points, or conformation of the polymer fiber generated in the electrospinning process.[33] When cyclically loaded for 1000 cycles, the aromatic TPU membrane can still carry 38% of the original stress (Figure 5), while the aliphatic TPU membrane can continue to carry 50% of the original stress (Figure S8). Like PLA, some permanent deformation in the TPU membranes occurs from fiber slippage after multiple loading cycles. In applications where the membrane would be repeatedly stretched, such as facial garments, this increased cyclic durability over pure PLA membranes is advantageous.

Blending TPU and PLA solutions resulted in fibrous membranes with mechanical properties that bridged the gap between the pure PLA and TPU membranes. With increasing TPU concentration, the elongation at break increased, while the stiffness decreased. For both aromatic and aliphatic TPU membranes, TPU20PLA80 still has a definitive yield point denoted by a sharp change in the slope of the tensile response, but at 50 wt % the membrane starts to behave like an elastomer. TPU80PLA20 has a combination of higher ultimate tensile stress paired with high elongation at break compared with pure membranes. An overview of mechanical properties for all blends of aromatic TPU, aliphatic TPU, and PLA are shown in Table 1. Across concentrations, the aromatic TPU blended with PLA had higher ultimate tensile strength (UTS) and elongation at the break. The TPU formulation and PLA ratio could be tuned based on application requirements.

*Biodegradation Testing.* All membranes were tested for their ability to biodegrade under home compost conditions. After 40 days of compost incubation, there is noticeable deterioration of the PLA100 fibers (Figure 6B). Even after as little as 20 days, pockmarks and the wearing of the PLA fibers can be observed (Figure 7B). Evidence showing that PLA degrades slowly at 36 °C has been previously reported.[6] Nevertheless, the PLA100 fibers had noticeable deterioration after 40 days, possibly due to a high surface-to-volume ratio. FTIR analysis demonstrates that this deterioration is occurring at the chemical level (Figure 6C). The addition of the O−H stretch peak (3291 cm$^{-1}$) and the decrease intensities in the C═O (1748 cm$^{-1}$) and C−O (1180 and 1080 cm$^{-1}$) ester stretch peaks suggest that the ester bonds within the PLA chain are undergoing hydrolysis, resulting in an increase in hydroxyl groups present in the sample.

At 40 days of compost incubation, the aromatic TPU fibers begin to agglomerate, which could facilitate the growth of microorganism populations and further degrade these membranes (Figure 6). In contrast, the aliphatic TPU membranes degraded at a macro level within 40 days (Figure S9) and showed signs of degradation under SEM in 20 days (Figure 7). The process of degradation It has been shown that hydrophobicity and hard segments in TPUs resist hydrolytic and enzymatic degradability.[29,30] The two aromatic rings from the MDI in the aromatic TPU membranes contribute to the hard segment of the urethane and likely contribute to its slower rate of degradation compared with the aliphatic TPU. Agglomeration of compost onto fibers and membranes that may include microorganisms can be seen on the membranes during degradation.

FTIR analysis provides further evidence of biodegradation of the aliphatic TPU membrane (Figure 7C). A marked increase in the O−H stretch peak (3319 cm$^{-1}$) and a decrease in the C═O stretch (1725 cm$^{-1}$), C−O stretch (1150 cm$^{-1}$), and C−O−C stretch (1036 cm$^{-1}$) peaks suggest that the ester bonds within the polyester urethane are undergoing ester cleavage resulting in an increase in diacid hydroxyl groups. This supports the claim that the polymer is biodegrading, as opposed to an alternate hypothesis such as disintegration through mechanical fragmentation. The same changes in peak intensities are observed in the aliphatic TPU and PLA blends (Figure S10). The ester bonds within both the TPU and PLA are broken, leading to more hydroxyl groups and less intact ester linkages within the polymer as biodegradation progresses. The compost pH was 7, as measured using a pH test strip. This neutral pH decreases the likelihood of acid- or base-catalyzed hydrolysis. Most likely, esterases excreted by microorganisms in the compost cleave these ester bonds to make the component molecules available to the microbes as nutrients.

When choosing between these two TPU formulations, there is a trade-off between mechanical strength and degradation speed. For applications in which rapid degradation is not as important as mechanical strength, aromatic TPU could be a good choice. Regardless of choice, both of these TPUs are derived from biobased sources, making them an attractive alternative to traditional petroleum-based TPUs.


https://doi.org/10.1021/acsapm.4c01974
ACS Appl. Polym. Mater. 2024, 6, 12528−12537

*Filtration Testing.* The difference in porosity between membranes becomes apparent when testing the filtration efficiency and pressure drop through the membranes (Figure 8). In the TPU100 and TPU80PLA20 membranes, the fibers are densely packed with small pore sizes, which results in a larger pressure drop. The more porous PLA100 and TPU20PLA80 had significantly lower pressure drops through the membrane. Both the fiber diameter and fiber density come together to influence the resistance of airflow through a membrane. Two air molecules can be separated by a mean spatial distance of 0.0034 $\mu$m at standard temperature ($T$ = 288 K). The collision of air molecules with each other and the surfaces of the fibers generates the drag forces that result in a pressure loss through the membrane.[34] The size of air molecules is orders of magnitude smaller than the particulate matter measured in the filtration efficiency experiment.

The filtration efficiency is associated with the membrane's ability to stop particulate matter within the air stream. In this experimental setup, burning tissue paper was used as the aerosol particle generator, and the sensor could sense particles above 2.5 $\mu$m in diameter. At a certain particle size, the higher porosity membranes will no longer be effective filtration media. The larger pore size would allow the smaller particulate matter to pass the membrane. All of the membranes tested in this study had pore sizes that effectively stopped particles above 2.5 $\mu$m, so the filtration efficiency for the tested porous membranes is near 100%. We expect to see the difference of filtration efficiency for the investigated porous membranes if the particle size is smaller. When evaluating the quality factor, the larger pressure drops decrease the quality factor. Additional work could be done to modify the electrospinning parameters to improve the pressure drop through the TPU100 and TPU80PLA20 membranes.

**Discussion.** Electrospun PLA membranes can be made more robust by blending with bioderived TPU. After 1000 tensile cycles to a strain of 50% the 50/50 blend still carries nearly 50% of the original stress. Much of the current literature does not report any cyclic testing of air filtration membranes, but many membranes will experience repeated loading in real-world applications such as the donning/doffing of face masks and deformations that occur during speech.

The filtration efficiency of 99% is comparable to that in the literature and higher than the requirement for N95, which means that it effectively filters out a minimum of 95% of airborne particles with a mass median aerodynamic diameter of 0.3 $\mu$m. Upon industrialization, this membrane could replace the filter media in the N95 masks. Table S1 contains an overview of the reported mechanical properties and filtration performance of previously published electrospun membranes.

The visual degradation observed in the biodegradation testing suggests that these membranes degrade well in a home compost environment. This qualitative measure of biodegradation is an improvement over studies of PLA and other biobased air filters that claim to be biodegradable but do not show any supporting results and previous reports that PLA is not biodegradable in environments with temperatures lower than those used in industrial composting. The FTIR spectra show the addition of the hydroxyl peak and decreased intensity of ester peaks after compost burial support bond cleavage, rather than abiotic degradation mechanisms such as fragmentation. The lack of visual degradation in the aromatic TPU membrane does not dispel biodegradation, but the rate is slower than both the aliphatic TPU and PLA. Other studies have shown the biodegradation of polyurethane synthesized from MDI and linear polyester polyols in both marine and soil environments.[35,36] Aromatic moieties as well as hard segment concentration have both been shown to slow biodegradation.[29,30]

A further improvement of biodegradation testing would be a measurement of respirometry of the compost environment.[27] A respirometer measures the rate of respiration or metabolic activity of microorganisms present in a sample. In the context of plastic degradation, respirometry can be used to monitor the microbial activity involved in the biodegradation process. As microorganisms break down plastic materials, they consume oxygen and produce carbon dioxide, water, and other byproducts. By measuring changes in oxygen consumption or carbon dioxide production over time using a respirometer, researchers can infer the rate and extent of plastic degradation by microbial activity. This provides conclusive evidence of plastic mineralization by microbes. A TPU very similar to the aliphatic TPU from this work has been proven to biodegrade in compost with respirometry.[37] This material reached over 75% theoretical biodegradation in 150 days. This study isolated bacterial strains called *Rhodococcus* and *Pseudomonas* that are exceptionally efficient at depolymerizing aliphatic polyester urethane. Future work could include a more quantitative study of membrane biodegradation in other natural environments (marine, freshwater, soil, etc.).

## CONCLUSIONS

Blending PLA and bioderived TPU offer a sustainable substitute for conventional membranes made from nonrenewable resources, meeting the requirements for a N95 face mask. This environmentally friendly membrane visually degrades in 40 days in compost, suggesting good biodegradability. Through testing of the membrane's mechanical strength via tensile and cyclic testing, the membrane demonstrated its durability and suitability for real-world usage.

While air filtration is mentioned as a potential application, further research could explore other potential uses for PLA/TPU membranes. This could involve investigating its suitability in diverse fields such as water filtration, medical applications, packaging, and energy storage, among others. Assessing its performance and compatibility in these different contexts would help expand its potential market applications.

## ASSOCIATED CONTENT

### Supporting Information

The Supporting Information is available free of charge at https://pubs.acs.org/doi/10.1021/acsapm.4c01974.

Gel permeation chromatography (GPC) curve of biobased aromatic TPU (Figure S1); $^{1}$H NMR of bio-based aromatic TPU in DMSO-$d_6$ (Figure S2); $^{13}$C NMR of bio-based aromatic TPU in DMSO-$d_6$ (Figure S3); stress-strain results of bio-based TPUs (Figure S4); differential scanning calorimetry (DSC) analysis of bio-based aromatic TPU (Figure S5); tensile results of PLA and aromatic TPU blends (Figure S6); tensile results of aliphatic TPU blends (Figure S7); cyclic testing of PLA and aliphatic TPU blends (Figure S8); optical images of PLA and aliphatic TPU blends degradation (Figure S9); FTIR spectra of aliphatic TPU and PLA blends after compost burial (Figure S10); and comparison of mechanical and filtration performance of electrospun membranes (Table S1) (PDF)



https://doi.org/10.1021/acsapm.4c01974
ACS Appl. Polym. Mater. 2024, 6, 12528−12537

This movie demonstrates the biodegradability of the aliphatic TPU membrane in compost over a 12 day span (MP4)

## AUTHOR INFORMATION


### Corresponding Author

**Shengqiang Cai** − *Material Science and Engineering Department, University of California, San Diego, La Jolla, California 92093, United States;* orcid.org/0000-0002-6852-7680; Email: shqcai@ucsd.edu

### Authors

**Robert J. Chambers** − *Material Science and Engineering Department, University of California, San Diego, La Jolla, California 92093, United States;* orcid.org/0000-0001-8475-4501

**Bhausaheb S. Rajput** − *Department of Chemistry and Biochemistry, University of California, San Diego, La Jolla, California 92093, United States*

**Gordon B. Scofield** − *Algenesis Corporation, San Diego, California 92121, United States;* orcid.org/0009-0009-2492-7381

**Jaysen Reindel** − *Algenesis Corporation, San Diego, California 92121, United States;* orcid.org/0009-0006-5137-0927

**Katherine O'Shea** − *Algenesis Corporation, San Diego, California 92121, United States;* orcid.org/0009-0009-5368-4761

**Richey Jiang Li** − *Material Science and Engineering Department, University of California, San Diego, La Jolla, California 92093, United States;* orcid.org/0000-0001-9387-2235

**Ryan Simkovsky** − *Algenesis Corporation, San Diego, California 92121, United States;* orcid.org/0000-0001-6837-0460

**Stephen P. Mayfield** − *Department of Molecular Biology, California Center for Algae Biotechnology, University of California, San Diego, La Jolla, California 92093, United States;* orcid.org/0000-0001-7642-9047

**Michael D. Burkart** − *Department of Chemistry and Biochemistry, University of California, San Diego, La Jolla, California 92093, United States;* orcid.org/0000-0002-4472-2254

Complete contact information is available at: https://pubs.acs.org/10.1021/acsapm.4c01974


### Author Contributions

The manuscript was written through the contributions of all the authors. All the authors have approved the final version of the manuscript.

### Notes

The authors declare the following competing financial interest(s): G.B.S., J.R., R.S., and K.O. are employees and shareholders in Algenesis Corporation, a company that could benefit from this research. M.D.B. and S.P.M. are founders and hold an equity position in Algenesis Corporation.

## ACKNOWLEDGMENTS

The authors acknowledge the support of the National Science Foundation through grant no. CMMI-2029145 and grant no. DMR-2011924. The microscopy was performed in part at the San Diego Nanotechnology Infrastructure (SDNI) of UC San Diego, a member of the National Nanotechnology Coordinated Infrastructure (NNCI), which is supported by the National Science Foundation. The authors acknowledge the use of facilities and instrumentation supported by NSF through the UC San Diego Materials Research Science and Engineering Center (UCSD MRSEC), grant # DMR-2011924.

## REFERENCES


(1) IEA CO2 Emissions in 2022, 2023. https://www.iea.org/reports/co2-emissions-in-2022.

(2) Geyer, R.; Jambeck, J. R.; Law, K. L. Production, use, and fate of all plastics ever made. *Sci. Adv.* **2017**, *3*, No. e1700782, DOI: 10.1126/sciadv.1700782.

(3) Lebreton, L.; Slat, B.; Ferrari, F.; et al. Evidence that the Great Pacific Garbage Patch is rapidly accumulating plastic. *Sci. Rep.* **2018**, *8*, 4666.

(4) Rosenboom, J.-G.; Langer, R.; Traverso, G. Bioplastics for a circular economy. *Nat. Rev. Mater.* **2022**, *7*, 117−137.

(5) Purkiss, D.; Allison, A. L.; Lorencatto, F.; Michie, S.; Miodownik, M. Big Compost Experiment: Using citizen science to assess the impact and effectiveness of biodegradable and compostable plastics in UK home composting. *Front. Sustain.* **2022**, *3*, No. 942724.

(6) García-Depraect, O.; Lebrero, R.; Rodriguez-Vega, S.; Bordel, S.; Santos-Beneit, F.; Martínez-Mendoza, L. J.; Börner, R. A.; Börner, T.; Muñoz, R. Biodegradation of bioplastics under aerobic and anaerobic aqueous conditions: Kinetics, carbon fate and particle size effect. *Bioresour. Technol.* **2022**, *344*, No. 126265.

(7) Royer, S.-J.; Greco, F.; Kogler, M.; Deheyn, D. D. Not so biodegradable: Polylactic acid and cellulose/plastic blend textiles lack fast biodegradation in marine waters. *PLoS One* **2023**, *18*, No. e0284681.

(8) Aragaw, T. A. Surgical face masks as a potential source for microplastic pollution in the COVID-19 scenario. *Mar. Pollut. Bull.* **2020**, *159*, No. 111517.

(9) Zhang, X.; Ru, Z.; Sun, Y.; Zhang, M.; Wang, J.; Ge, M.; Liu, H.; Wu, S.; Cao, C.; Ren, X.; Mi, J.; Feng, Y. Recent advances in applications for air pollutants purification and perspectives of electrospun nanofibers. *J. Cleaner Prod.* **2022**, *378*, No. 134567.

(10) Lyu, C.; Zhao, P.; Xie, J.; Dong, S.; Liu, J.; Rao, C.; Fu, J. Electrospinning of Nanofibrous Membrane and Its Applications in Air Filtration: A Review. *Nanomaterials* **2021**, *11*, 1501.

(11) Samatya Yılmaz, S.; Aytac, A. The highly absorbent polyurethane/polylactic acid blend electrospun tissue scaffold for dermal wound dressing. *Polym. Bull.* **2023**, *80*, 12787−12813.

(12) Francis, L.; Ahmed, F. E.; Hilal, N. Electrospun membranes for membrane distillation: The state of play and recent advances. *Desalination* **2022**, *526*, No. 115511.

(13) Liu, C.; Hsu, P.-C.; Lee, H.-W.; Ye, M.; Zheng, G.; Liu, N.; Li, W.; Cui, Y. Transparent air filter for high-efficiency PM2.5 capture. *Nat. Commun.* **2015**, *6*, No. 6205.

(14) Deng, Y.; Lu, T.; Cui, J.; Samal, S. K.; Xiong, R.; Huang, C. Bio-based electrospun nanofiber as building blocks for a novel eco-friendly air filtration membrane: A review. *Sep. Purif. Technol.* **2021**, *277*, No. 119623.

(15) Wang, J.; Liu, S.; Yan, X.; Jiang, Z.; Zhou, Z.; Liu, J.; Han, G.; Ben, H.; Jiang, W. Biodegradable and Reusable Cellulose-Based Nanofiber Membrane Preparation for Mask Filter by Electrospinning. *Membranes* **2022**, *12*, 23.

(16) He, H.; Gao, M.; Illés, B.; Molnar, K. 3D Printed and Electrospun, Transparent, Hierarchical Polylactic Acid Mask Nanoporous Filter. *Int. J. Bioprint.* **2020**, *6* (4), No. 278, DOI: 10.18063/ijb.v6i4.278.

(17) Han, W.; Rao, D.; Gao, H.; Yang, X.; Fan, H.; Li, C.; Dong, L.; Meng, H. Green-solvent-processable biodegradable poly(lactic acid) nanofibrous membranes with bead-on-string structure for effective air filtration: "Kill two birds with one stone". *Nano Energy* **2022**, *97*, No. 107237.

(18) Wang, L.; Gao, Y.; Xiong, J.; Shao, W.; Cui, C.; Sun, N.; Zhang, Y.; Chang, S.; Han, P.; Liu, F.; He, J. Biodegradable and high-

performance multiscale structured nanofiber membrane as mask filter media via poly(lactic acid) electrospinning. *J. Colloid Interface Sci.* **2022**, *606*, 961−970.
(19) Liu, Y.; Wei, H.; Wang, Z.; Li, Q.; Tian, N. Simultaneous Enhancement of Strength and Toughness of PLA Induced by Miscibility Variation with PVA. *Polymers* **2018**, *10*, No. 1178.
(20) Shi, Q.; Zhou, C.; Yue, Y.; Guo, W.; Wu, Y.; Wu, Q. Mechanical properties and in vitro degradation of electrospun bio-nanocomposite mats from PLA and cellulose nanocrystals. *Carbohydr. Polym.* **2012**, *90*, 301−308.
(21) Samatya Yilmaz, S.; Aytac, A. Poly(lactic acid)/polyurethane blend electrospun fibers: structural, thermal, mechanical and surface properties. *Iran. Polym. J.* **2021**, *30*, 873−883.
(22) Wu, Z.; Zhang, Z.; Wei, W.; Yin, Y.; Huang, C.; Ding, J.; Duan, Q. Investigation of a novel poly (lactic acid) porous material toughened by thermoplastic polyurethane. *J. Mater. Sci.* **2022**, *57*, 5456−5466.
(23) Chen, R.; Zhang, X.; Wang, P.; Xie, K.; Jian, J.; Zhang, Y.; Zhang, J.; Yuan, Y.; Na, P.; Yi, M.; Xu, J. Transparent thermoplastic polyurethane air filters for efficient electrostatic capture of particulate matter pollutants. *Nanotechnology* **2019**, *30*, No. 015703.
(24) Liang, W.; Xu, Y.; Li, X.; Wang, X.-X.; Zhang, H.-D.; Yu, M.; Ramakrishna, S.; Long, Y.-Z. Transparent Polyurethane Nanofiber Air Filter for High-Efficiency PM2.5 Capture. *Nanoscale Res. Lett.* **2019**, *14*, 361.
(25) Niu, Z.; He, Q.; Chen, C. A PM2.5 Pollution-Level Adaptive Air Filtration System based on Elastic Filters for Reducing Energy Consumption. *J. Hazard. Mater.* **2024**, *478*, No. 135546.
(26) Rajput, B. S.; Hai, T. A. P.; Burkart, M. D. High Bio-Content Thermoplastic Polyurethanes from Azelaic Acid. *Molecules* **2022**, *27*, 4885.
(27) Rajput, B. S.; Hai, T. A. P.; Gunawan, N. R.; Tessman, M.; Neelakantan, N.; Scofield, G. B.; Brizuela, J.; Samoylov, A. A.; Modi, M.; Shepherd, J.; Patel, A.; Pomeroy, R. S.; Pourahmady, N.; Mayfield, S. P.; Burkart, M. D. Renewable low viscosity polyester-polyols for biodegradable thermoplastic polyurethanes. *J. Appl. Polym. Sci.* **2022**, *139*, No. e53062.
(28) Branson, Y.; Söltl, S.; Buchmann, C.; Wei, R.; Schaffert, L.; Badenhorst, C. P. S.; Reisky, L.; Jäger, G.; Bornscheuer, U. Urethanases for the enzymatic hydrolysis of low molecular weight carbamates and the recycling of polyurethanes. *Angew. Chem., Int. Ed.* **2023**, *62*, No. e202216220.
(29) Umare, S. S.; Chandure, A. S. Synthesis, characterization and biodegradation studies of poly(ester urethane)s. *Chem. Eng. J.* **2008**, *142*, 65−77.
(30) Pfohl, P.; Bahl, D.; Rückel, M.; Wagner, M.; Meyer, L.; Bolduan, P.; Battagliarin, G.; Hüffer, T.; Zumstein, M.; Hofmann, T.; Wohlleben, W. Effect of Polymer Properties on the Biodegradation of Polyurethane Microplastics. *Environ. Sci. Technol.* **2022**, *56*, 16873−16884.
(31) Thompson, C.; Chase, G.; Yarin, A.; Reneker, D. Effects of parameters on nanofiber diameter determined from electrospinning model. *Polymer* **2007**, *48*, 6913−6922.
(32) Negi, V.; Picu, R. C. Mechanical behavior of nonwoven non-crosslinked fibrous mats with adhesion and friction. *Soft Matter* **2019**, *15*, 5951−5964.
(33) Baji, A.; Mai, Y.-W.; Wong, S.-C.; Abtahi, M.; Chen, P. Electrospinning of polymer nanofibers: Effects on oriented morphology, structures and tensile properties. *Compos. Sci. Technol.* **2010**, *70*, 703−718.
(34) Zhao, X.; Wang, S.; Yin, X.; Yu, J.; Ding, B. Slip-Effect Functional Air Filter for Efficient Purification of PM2.5. *Sci. Rep.* **2016**, *6*, No. 35472.
(35) Gunawan, N. R.; Tessman, M.; Schreiman, A. C.; Simkovsky, R.; Samoylov, A. A.; Neelakantan, N. K.; Bemis, T. A.; Burkart, M. D.; Pomeroy, R. S.; Mayfield, S. P. Rapid biodegradation of renewable polyurethane foams with identification of associated microorganisms and decomposition products. *Bioresour. Technol. Rep.* **2020**, *11*, No. 100513.
(36) Gunawan, N. R.; Tessman, M.; Zhen, D.; Johnson, L.; Evans, P.; Clements, S. M.; Pomeroy, R. S.; Burkart, M. D.; Simkovsky, R.; Mayfield, S. P. Biodegradation of renewable polyurethane foams in marine environments occurs through depolymerization by marine microorganisms. *Sci. Total Environ.* **2022**, *850*, No. 158761.
(37) Allemann, M. N.; Tessman, M.; Scofield, G. B.; Evans, P.; Pomeroy, R. S.; Burkart, M. D.; et al. Rapid biodegradation of microplastics generated from bio-based thermoplastic polyurethane. *Sci. Rep.* **2024**, *14*, No. 6036, DOI: 10.1038/s41598-024-56492-6.